Geological Society of America
Field Guide 6
2005

Brittle deformation, fluid flow, and diagenesis in sandstone at Valley of Fire State Park, Nevada

Peter Eichhubl
Texas A&M University-Corpus Christi, Corpus Christi, Texas 78412, USA

Eric Flodin
Indiana University–Purdue University, Fort Wayne, Indiana 46805, USA

ABSTRACT

The interaction among brittle deformation, fluid flow, and diagenesis is displayed at Valley of Fire, southern Nevada, where diagenetic iron oxide and hydroxide stains provided a visible record of paleofluid flow in Jurassic Aztec Sandstone. Deformation features include deformation bands, joints, and faults composed of deformation bands and sheared joints. Faults formed by shear along joints, formation of splay fractures, and linkage of fault segments. Measurements of fault permeability, combined with numerical permeability upscaling, indicate that these faults impede cross-fault fluid flow, with cross-fault permeability reduced by two orders of magnitude relative to the host sandstone, whereas fault-parallel permeability is enhanced by nearly one order of magnitude.

A reconstruction of paleofluid flow in the Aztec Sandstone is based on detailed mapping of multicolored alteration patterns and their cross-cutting relations with brittle structures. These patterns resulted from syndepositional reddening of the eolian sandstone and repeated episodes of dissolution, mobilization, and reprecipitation of iron oxide and hydroxide. The distribution of alteration patterns indicates that regional-scale fluid migration pathways were controlled by stratigraphic contacts, thrust faults, and high-angle oblique-slip faults. Outcrop-scale focusing of fluid flow was controlled by structural heterogeneities such as joints, joint-based faults, and deformation bands as well as the sedimentary architecture. The complex interaction of structural heterogeneities with alteration in this exhumed analog of a fractured and faulted sandstone aquifer is consistent with their measured hydraulic properties demonstrating the significance of structural heterogeneities for focused fluid flow in porous sandstone aquifers.

Keywords: fluid flow, sandstone, diagenesis, faults and faulting, jointing, permeability.

INTRODUCTION

Brittle deformation, fluid flow, and diagenetic processes are coupled phenomena (Dickinson and Milliken, 1995; Eichhubl and Behl, 1998; Laubach et al., 2004; Eichhubl et al., 2004; Gale et al., 2004). Brittle structures such as joints, deformation bands, and faults composed of joints and deformation bands affect fluid flow and thus mass transfer and chemical alteration in the subsurface (Antonellini and Aydin, 1994; Eichhubl and Boles, 2000; Flodin et al., 2005). Diagenetic processes such as compaction, grain dis-

Eichhubl, P., and Flodin, E., 2005, Brittle deformation, fluid flow, and diagenesis in sandstone at Valley of Fire State Park, Nevada, *in* Pederson, J., and Dehler, C.M., eds., Interior Western United States: Geological Society of America Field Guide 6, p. 151–167, doi: 10.1130/2005.fld006(07).

solution, and cementation affect the physical properties of rock and thus the deformation behavior (Gross, 1995; Flodin et al., 2003).

This field trip examines the interaction among these processes in an exhumed sandstone aquifer at Valley of Fire State Park, located in the Northern Muddy Mountains along the shores of Lake Mead, ~60 km northwest of Las Vegas, Nevada (Fig. 1). The Northern Muddy Mountains are part of the Basin and Range physiographic province, located ~50 km west of the western edge of the Colorado Plateau. The park also contains a frontal section of the Sevier orogenic belt of Cretaceous age. This trip is dedicated to the interplay among depositional architecture, Cretaceous and Tertiary deformation, fluid flow, and chemical mass transfer.

STRATIGRAPHY OF VALLEY OF FIRE

The name of the park relates to the red, purple, orange, yellow, and white hues of the Upper Triassic and Jurassic Aztec Sandstone (Bohannon, 1977, 1983). This eolian sandstone was deposited in a backarc setting (Marzolf, 1983, 1990) and is considered equivalent to the Navajo Sandstone of the Colorado Plateau and the Nugget Sandstone in the Wyoming thrust belt (Poole, 1964; Blakey, 1989). The Aztec Sandstone at Valley of Fire is part of a Mesozoic clastic sequence that overlies Upper Paleozoic carbonates and shale (Bohannon, 1983). Triassic redbeds of the Moenkopi, Chinle, and Moenave Formations, with a combined thickness of up to 2100 m (Bohannon, 1977), are composed of sand-, silt-, and mudstone with evaporite layers (Marzolf, 1990). The Aztec Sandstone is unconformably overlain, with a discordance of locally up to 10°, by a distinctive conglomerate that forms the basal member of the Cretaceous Willow Tank Formation. The Willow Tank Formation, composed of predominantly mudstone, and the overlying Baseline Sandstone have a combined thickness of ~1300 m (Bohannon, 1977). These units are interpreted as synorogenic foreland deposits of the eastward-directed Cretaceous Sevier thrust sheets (Bohannon, 1983). The basal conglomerate of the Willow Tank Formation includes locally derived red Aztec sandstone components (Longwell, 1949), indicative of partial exhumation and erosion of the Aztec Sandstone subsequent to its deposition (Bohannon, 1983).

The Willow Tank Formation and lower portions of the Cretaceous Baseline Sandstone are overthrust by Aztec Sandstone of the Willow Tank thrust sheet (Fig. 2), the lowest of the Sevier thrust sheets in Valley of Fire (Longwell, 1949; Bohannon, 1983). Tearfault Mesa in the northern part of Figure 2 forms a klippe of the Willow Tank thrust sheet. Cretaceous strata are steepened and locally overturned along the eastern margin of this klippe (Longwell, 1949), indicating that the eastern edge of the klippe represents the leading edge of the thrust sheet. Upper portions of the Baseline Sandstone are deposited on top of the Willow Tank thrust sheet, constraining the age of thrusting to Late Cretaceous (Maastrichtian) (Longwell, 1949; Bohannon, 1983).

After a hiatus during Paleogene times, conformable deposition of clastic units resumed during Oligocene times (Bohannon, 1983). A ~25° angular unconformity at the base of the Upper Miocene (10–4 Ma) Muddy Creek Formation (Bohannon et al., 1993) constrains the time of regional tilting of the Aztec Sandstone, presently dipping 20–30° NE in the area visited on this trip (Fig. 2). The Muddy Creek Formation, in turn, dips 5–8° NE, indicating continued regional tilting throughout the Late Miocene. The Aztec Sandstone and overlying Cretaceous strata are folded into a gentle NE-plunging syncline referred to as Overton syncline by Carpenter and Carpenter (1994) (Fig. 2).

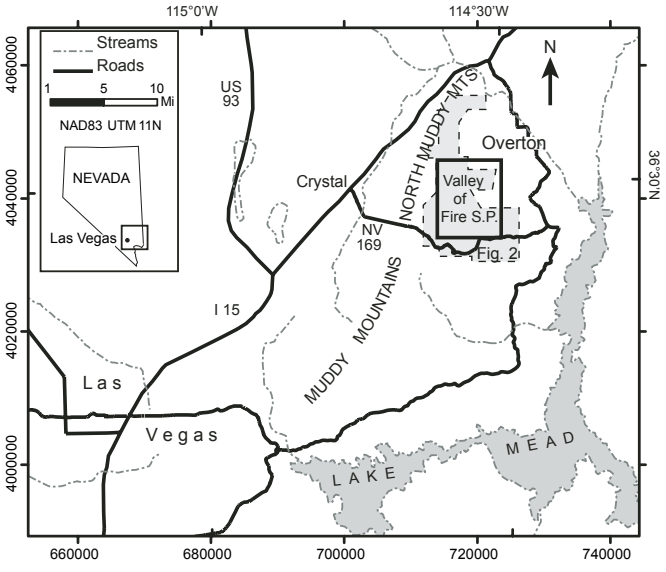

Figure 1. Location of map of Valley of Fire State Park in southern Nevada.

DEFORMATION OF THE AZTEC SANDSTONE

Deformation structures in the Aztec Sandstone include deformation bands, joints and sheared joints, and faults that are composed of deformation bands, slip surfaces, sheared joints, and breccia zones.

Deformation bands are tabular zones of localized deformation that are frequently more resistant to erosion. Thus, they are often observed on the outcrop as ridges ranging in thickness from 1 mm to 10 cm, with a typical width of ~1 cm (Antonellini and Aydin, 1994). At Valley of Fire, Hill (1989) distinguished three earlier sets of deformation bands, striking northwest, north-northwest, and north-northeast, that are characterized by predominant band-parallel compaction. Following Mollema and Antonellini (1996) and Sternlof and Pollard (2001), we refer to these deformation bands as compaction bands. Repeated mutual cross-cutting suggests that these three sets formed concurrently. These three sets of compaction bands are cross-cut by three sets of deformation bands (Flodin and Aydin, 2004) that exhibit macroscopic shear offsets and are therefore referred to as shear bands. One set of shear bands, with slip ranging from 1 to 3 cm, parallels

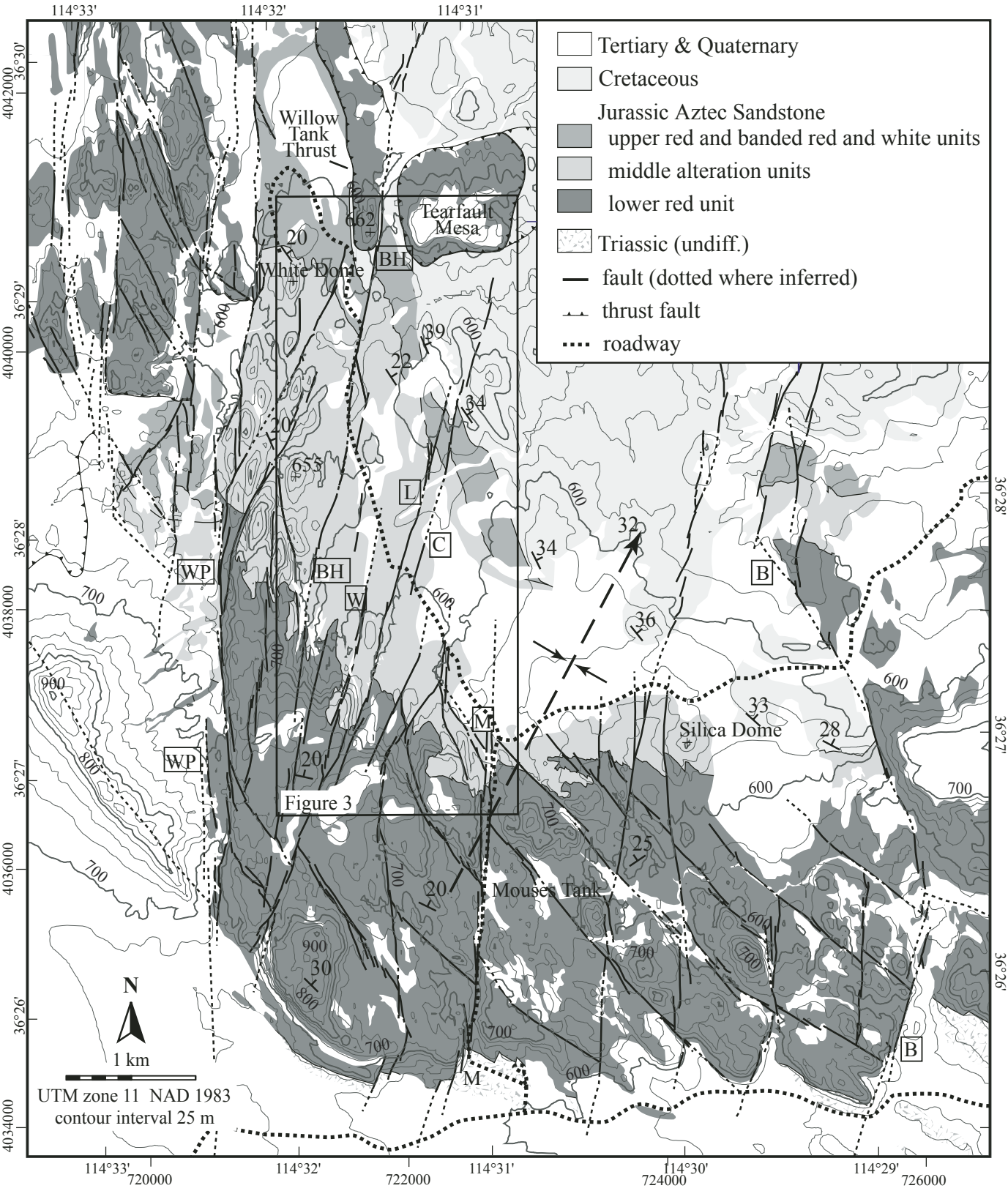

Figure 2. Geologic map of the northern part of Valley of Fire State Park. WP—Waterpocket fault; BH—Bighorn fault; W—Wall fault; L—Lone-wolf fault; C—Classic fault; M—Mouses Tank fault; B—Baseline fault. Figure from Eichhubl et al. (2004).

depositional boundaries of the cross-bedded strata (Hill, 1989). The other two sets of shear bands usually occur as subvertical zones of multiple shear bands and associated slip surfaces, with slip on the order of 1–10 cm (Flodin and Aydin, 2004). The top-to-the-east sense of shear of the bed-parallel shear bands is kinematically consistent with Sevier thrusting, suggesting that these shear bands formed concurrently with thrusting (Hill, 1989).

Taylor et al. (1999) distinguished four sets of joints in the Aztec Sandstone. The first set is composed of parallel vertical joints that strike roughly north-south. This set is locally replaced by two sets of joints that also strike north-south but form two intersecting sets with an acute angle of ~30°. Joints of the fourth set are slightly sinuous and do not show a strong preferred orientation, but may favor a roughly east-west orientation. Joints have been observed to consistently crosscut compaction and shear bands and are thus interpreted to form after deformation bands and concurrently with, and possibly also prior to, strike-slip faulting (Myers, 1999; Flodin and Aydin, 2004).

Two sets of oblique-slip faults with predominant strike-slip and lesser normal-slip components occur as two sets: a left-lateral fault set striking NNE, and a right-lateral set striking NW (Myers, 1999; Taylor, 1999; Flodin and Aydin, 2004) (Fig. 2). The NNE-striking set is more prominently developed on the regional scale, but both sets show mutually abutting geometries on a local scale, suggesting that both sets were active concurrently (Flodin and Aydin, 2004). This network of faults within the Valley of Fire is bounded by the Waterpocket fault system to the west and the Baseline fault system to the east (Fig. 2). Both the Waterpocket and Baseline fault systems show nearly 2.5 km of apparent left-lateral separation. They appear to be part of a larger family of ~N-trending left-lateral faults that occur to the northeast along Weiser Ridge and to the north in the southern and eastern Mormon Mountains and the Tule Spring Hills (Bohannon, 1992; Anderson and Barnhard, 1993; Axen, 1993).

These faults offset the Aztec–Willow Tank formation contact. Following the maps of Bohannon (1977) and Carpenter (1989), the youngest strata offset by faults of the Baseline fault system are the Miocene Horse Spring Formation and probably lower sections of the Upper Miocene Muddy Creek Formation (10–4 Ma; Bohannon et al., 1993). These faults are thus considered to be associated with Basin and Range tectonics (Flodin and Aydin, 2004).

DIAGENESIS OF AZTEC SANDSTONE

The Aztec Sandstone is a fine- to medium-grained subarkose (Marzolf, 1983) with up to 8% feldspar (Flodin et al., 2003) and a smaller amount of lithic components. The sandstone is generally friable with a porosity of 15%–25% and permeability of 100–2500 md (Flodin et al., 2003). Grains are subrounded to rounded, characteristic of the eolian depositional environment. Grains are weakly indented throughout the section as a result of pressure solution, and pore space is partially filled with clay cement, predominantly kaolinite and lesser mixed-layer illite-smectite. The mixed-layer illite-smectite is 90% illite with a Reichweite of 3. In the stratigraphically lowest part of the Aztec Sandstone, illite replaces the mixed-layer illite-smectite (Eichhubl et al., 2004).

Minor amounts of quartz overgrowth cement were observed in stratigraphically lower parts of the Aztec Sandstone. Quartz cement was also found locally within the damage zone and to both sides of the Bighorn fault (Fig. 2), cementing allochthonous Aztec Sandstone of the Willow Tank thrust sheet as well as fault rock that is part of the autochthonous Aztec Sandstone.

We estimate that the maximum burial depth at the top of the Aztec Sandstone corresponds closely to the thickness of the post-Jurassic units to the east, amounting to ~1600 m (based on stratigraphic thicknesses provided by Bohannon, 1983). The occurrence of quartz overgrowth cement and diagenetic illite in the lowermost part of the Aztec Sandstone, typically requiring burial temperatures in excess of ~80 °C (Worden and Morad, 2000, 2003), appears in agreement with this estimate. The geothermal gradient could have been elevated along the thrust front due to fluid flow, consistent with the occurrence of quartz cement along and below the Willow Tank thrust sheet.

The characteristic hues of red, orange, purple, yellow, and white of the Aztec Sandstone result from varying amounts and forms of iron oxide and hydroxide cement, the dominant pigments being hematite and goethite. The uniform red color of the lower red and upper red alteration units of the Aztec Sandstone results from thin grain coats of hematite. In thin section, hematite forms a mottled brownish coloration of grain surfaces. In samples of lower red sandstone containing quartz overgrowth cement, the hematite coat predates the quartz overgrowth, indicative of an early diagenetic or syndepositional origin of the hematite coat.

Compared to grain coats in red sandstone, grain coats in yellow sandstone (Munsell 10YR 7/6 yellow to 10YR 8/2 very pale brown; Munsell Soil Color Charts, 1994) are more patchy and partly recrystallized to ≤1-µm-sized crystals. Based on X-ray diffractograms, the dominant Fe-oxide is goethite. In orange-colored sandstone (Munsell 2.5 YR 5/8 red), hematite forms 5–10-µm-sized globules that are attached to grain surfaces. The equally spaced distribution of hematite globules along grain surfaces is suggestive of globule formation by local dissolution of earlier grain coats and reprecipitation of hematite with accompanying crystal coarsening. Purple coloration (Rock Color Chart 5RP 6/2 pale red purple to 5RP 4/2 grayish red purple, Rock-Color Chart Committee, 1970; and Munsell 10R 6/3 pale red) is caused by 1–3-µm-sized grains of Fe-oxide, identified by X-ray diffraction to be dominantly goethite. Some samples of purple and yellow sandstone also contain smaller amounts of the sulfates alunite $KAl_3(SO_4)_2(OH)_6$ and jarosite $KFe_3(SO_4)_2(OH)_6$. Jarosite provides a mottled brownish color to the otherwise uniform yellow sandstone. White sandstone (Munsell 10YR 8/1–7.5YR 8/1 white) is devoid of grain coats but contains sparse flakes of coarse-crystalline hematite.

IMPACT OF STRUCTURES ON FLUID FLOW

The flow characteristics of faults formed by shearing of joints in Aztec Sandstone, Valley of Fire, have been discussed by Myers

(1999), Taylor (1999), Aydin (2000), Flodin et al. (2001), Jourde et al. (2002), Flodin and Aydin (2004), and Flodin et al. (2005). The faults impart a dual influence on flow behavior, where fine-grained fault rock or gouge at the core of the fault zone reduces cross-fault permeability, and joints and slightly sheared joints in the surrounding fault-damage zone increase along-fault permeability. These flow properties correspond to a combined barrier-conduit system according to Caine et al. (1996).

Considering cross-fault permeability, Flodin et al. (2005) described petrophysical properties for a suite of fault rocks. They found an average permeability reduction of three orders of magnitude in fault-rock samples with respect to host-rock samples and that overall cross-fault permeability decreases with increasing average shear strain. Taylor et al. (1999) used numerical simulations to calculate flow fields perturbed by the presence of joints and sheared joints. By comparing their numerical results with field relationships, they estimated permeabilities for joints and slightly sheared joints in the Valley of Fire to be about five orders of magnitude greater than hostrock permeability. Myers (1999), using power-averaging techniques, calculated upscaled permeabilities for a series of outcrop-scale fault maps. He found significant permeability anisotropy with ratios between along- and cross-fault permeability ranging from one to four orders of magnitude. Jourde et al. (2002) took a numerical approach to the same upscaling problem and demonstrated a reduction of fault-normal permeability by two orders of magnitude relative to the host rock permeability. Permeability parallel to the fault, on the other hand, was found to be increased by nearly one order of magnitude relative to the host rock due to the presence of connected joint networks with a preferred orientation parallel to the fault.

The flow characteristics of individual compaction bands in the Valley of Fire were addressed by Taylor and Pollard (2000). At a larger-scale of observation, Sternlof et al. (2004) investigated the combined flow effects of arrays of compaction bands. They considered three different characteristic deformation band array geometries—parallel, cross-hatch, and anastomosing—and concluded that all were capable of imparting up to two orders of magnitude permeability reduction and a corresponding increase in permeability anisotropy.

INTERACTIONS AMONG STRUCTURAL, FLUID FLOW, AND DIAGENETIC PROCESSES

Rock units of common alteration color were mapped (Eichhubl et al., 2004) as shown in Figure 3, distinguishing nine types of alteration based either on the dominant color (red, yellow, etc.) or a combination of two colors (e.g., banded orange-and-white, banded purple-and-yellow). Rock units of common alteration color will be addressed in the field as alteration bands or alteration units. A schematic composite cross section across the diagenetic alteration units of the Aztec Sandstone (Fig. 4) illustrates the upward succession of a lower red unit, overlain by middle purple, yellow, orange, and white alteration units, and capped by an upper red alteration unit. Although these alteration units roughly parallel the stratigraphy, we will see at several stops that alteration bands and contacts cut depositional boundaries and thus postdate deposition. These alteration bands and units are thus the result of diagenetic processes.

Based on diagenetic and structural cross-cutting relations, Eichhubl et al. (2004) distinguished three stages of alteration (Fig. 5): a first stage of syndepositional reddening of the sand or sandstone and two stages of dissolution or bleaching, iron remobilization, and reprecipitation of iron oxide and hydroxide. The first stage of bleaching and iron remobilization, precipitating dominantly hematite, is attributed to upward migration of reducing basinal fluid during and subsequent to Late Cretaceous Sevier thrusting and foreland deposition of clastic sediments. A second stage of bleaching and iron remobilization, precipitating predominantly goethite and minor iron sulfates, occurred during Miocene strike-slip faulting associated with Basin and Range tectonics. This second stage is explained by mixing of reducing sulfide-rich basinal fluid with meteoric water entering the aquifer.

By relating patterns of alteration to fluid flow, we can derive that regional-scale fluid migration pathways were largely controlled by stratigraphic contacts, thrust faults, and high-angle oblique-slip faults. The outcrop-scale focusing of flow was controlled by structural heterogeneities such as joints, joint-based faults, and deformation bands as well as the sedimentary architecture. Deformation bands tend to form alteration boundaries, suggesting they acted as baffles to subsurface fluid flow. Joints and sheared joints are frequently surrounded by halos of enhanced reddening or bleaching indicative of focused fluid flow along joints.

The interaction of structural heterogeneities with paleofluid flow as inferred using the diagenetic alteration record is consistent with their measured hydraulic properties and flow models. Taylor et al. (1999) compared the distribution of alteration halos around isolated and interconnected joints with computed flow patterns, emphasizing the importance of joint connectivity for fluid flow in sandstone of high matrix permeability such as the Aztec Sandstone.

The combined field, laboratory, and modeling evidence demonstrates the significance of structural heterogeneities for controlling fluid flow properties of porous sandstone aquifers. In addition to the depositional heterogeneity, structural features focus fluid flow and chemical alteration. On a regional scale, the diagenetic and structural record at Valley of Fire illustrates the coupling of tectonic, fluid flow, and alteration processes.

DESCRIPTION OF STOPS

All stops described here are located within Valley of Fire State Park, within a driving distance of 5.5 mi (9 km) from each other (Fig. 6). Stops 2–6 require some hiking over easy terrain, with hikes not exceeding 1.5 mi (2.4 km) roundtrip. Although described here as a continuous trip, a visit of all stops will require one and a half to two full days. Best times to visit are during spring and fall; average daytime highs exceed 105 °F (40 °C) in the months of July and August.

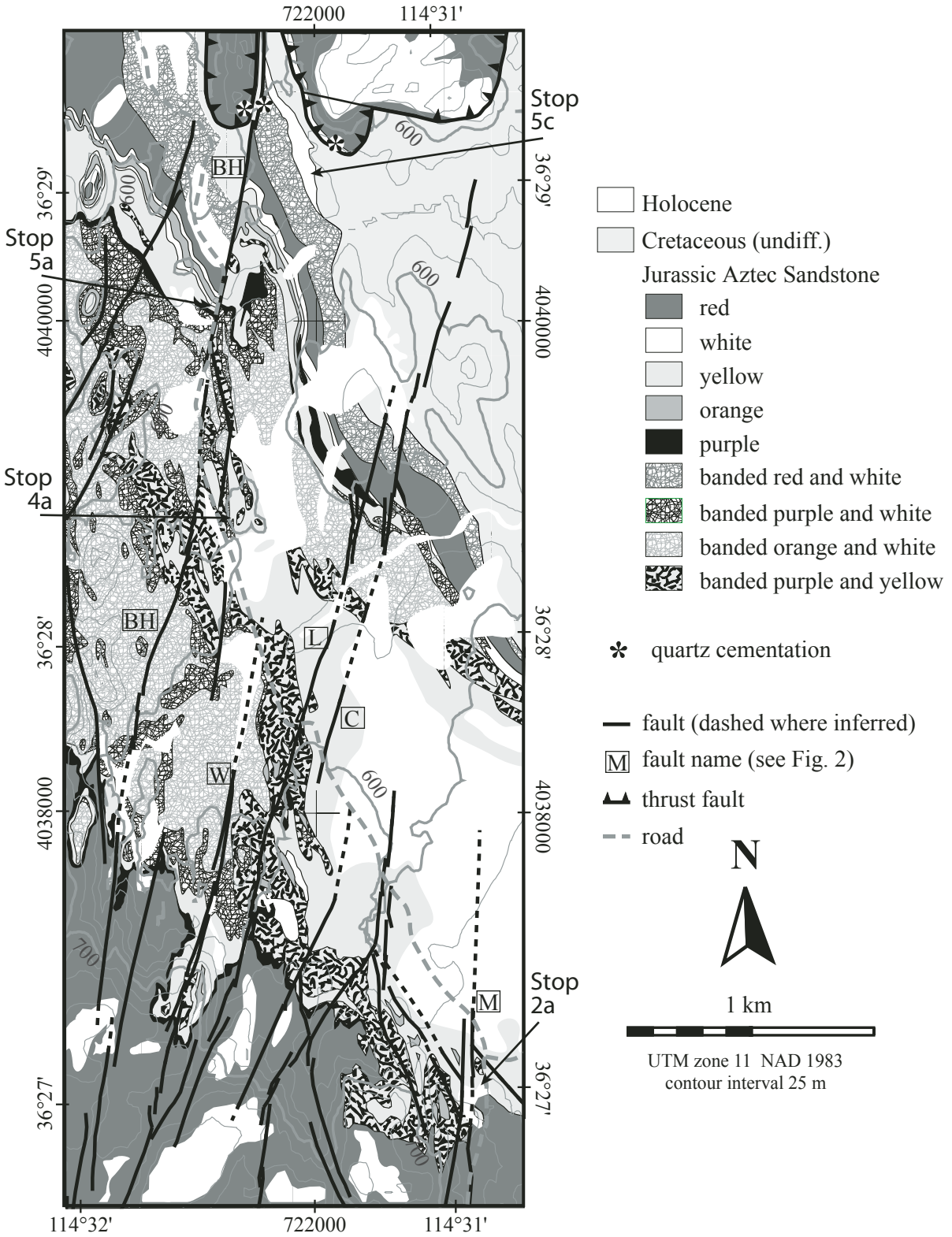

Figure 3. Map of diagenetic alteration units for area shown in Figure 2.

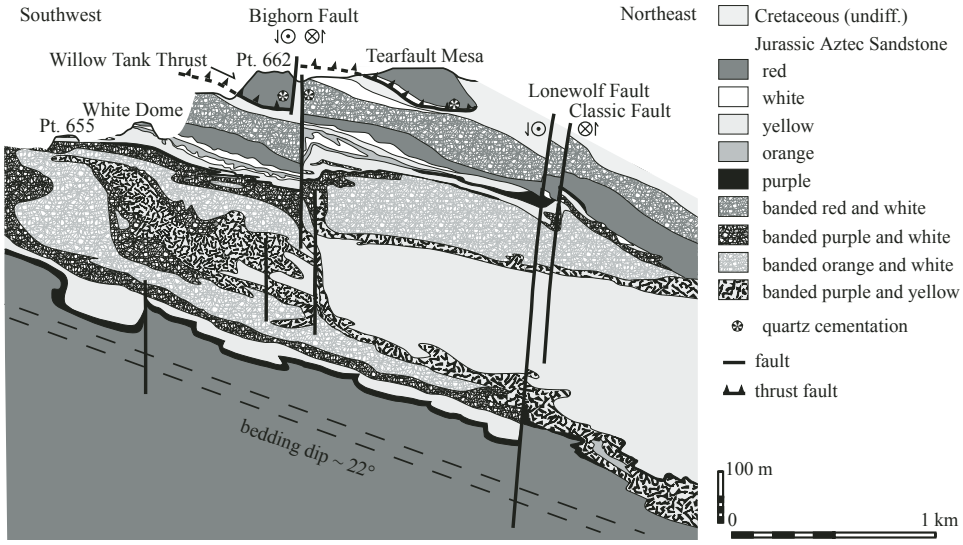

Figure 4. Schematic composite cross section across diagenetic alteration units in Figure 3, based on field sketches taken from several vantage points. Due to the northwestward plunge of the alteration units, the top parts of the section reflect observations in the northern portion of the map area, and lower parts are taken from observations in the southern portion of the map. Because alteration features do not project along strike over the extent of the map area, this section represents an idealized composite. Although unit thicknesses and inclination are approximately to scale, horizontal distances are condensed to about half of the vertical scale.

Directions to Stop 1

Valley of Fire State Park is accessed most conveniently from Las Vegas. Leave Las Vegas heading north on I-15, take Exit 75 at Crystal, and proceed on Nevada Route 169 southeast to Valley of Fire State Park. In the park, 18 mi (29 km) from I-15 Exit 75, turn left and park at the visitor's center (Stop 1). Park entrance fees are collected. Please note that sample collection is not permitted in Valley of Fire State Park without prior permission by the park administration. Parking is limited to designated parking areas.

Stop 1—Valley of Fire State Park Visitor's Center

The visitor's center provides a panoramic overlook of Valley of Fire Wash and the Muddy Mountains to the south. The wash follows the outcrop of less resistant Triassic sand- and siltstone units that underlie the cliff-forming Aztec Sandstone behind, and to the north of, the visitor's center. The visitor's center is situated on reddish sandstone and siltstone of the Upper Triassic Moenave Formation, with older Triassic Chinle and Moenkopi Formations underlying the central part of the wash. Red Aztec Sandstone is exposed in the lower parts of the Muddy Mountains to the south, including the Fire Alcove just to the south of our present position, as well as in the low hills in the upper part of Valley of Fire Wash (Atlatl Rock). The upper section of the Muddy Mountains is composed of Paleozoic limestone and dolostone, separated from the Mesozoic clastic units by the E-W–striking Arrowhead fault (Longwell, 1949).

Directions to Stop 2

Continue along the road that leads from the visitor's center into the northern part of the park. As the road climbs, we traverse from the Triassic red beds into the basal section of the Aztec Sandstone. The road enters a valley that follows the N-S–striking Mouses Tank fault. Continue past the Mouses Tank parking area and park at Rainbow Vista, 1.8 mi (2.9 km) from the visitor's center.

Stop 2a—Rainbow Vista

Following the road leading up from the visitor's center, we traversed the stratigraphically lower 800–900-m-thick section of the Aztec Sandstone. Apart from joint surfaces covered by dark-brown varnish, this section is characterized by a red stain that

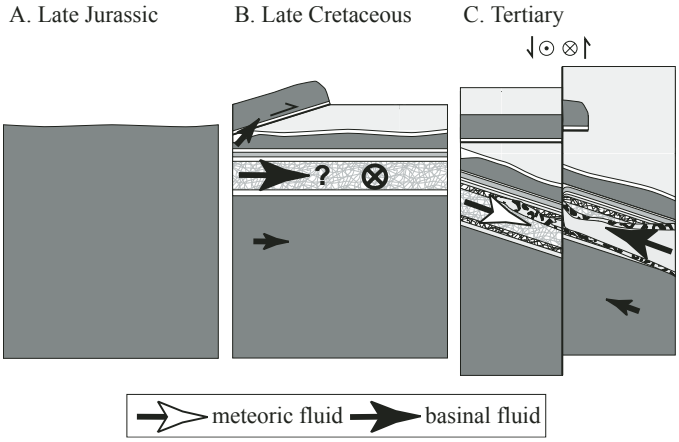

Figure 5. Stages of diagenetic alteration, fluid flow, and deformation in the Aztec Sandstone at Valley of Fire. (A) Syndepositional reddening of eolian sandstone. (B) First stage of bleaching and iron remobilization in upper section of the Aztec Sandstone associated with Sevier thrusting. Field observations suggest local flow along strike of the orogenic front, but a regional direction of flow away from the orogen is inferred. (C) Second stage of bleaching and iron remobilization associated with mixing of basinal and meteoric fluids during Basin and Range tectonics.

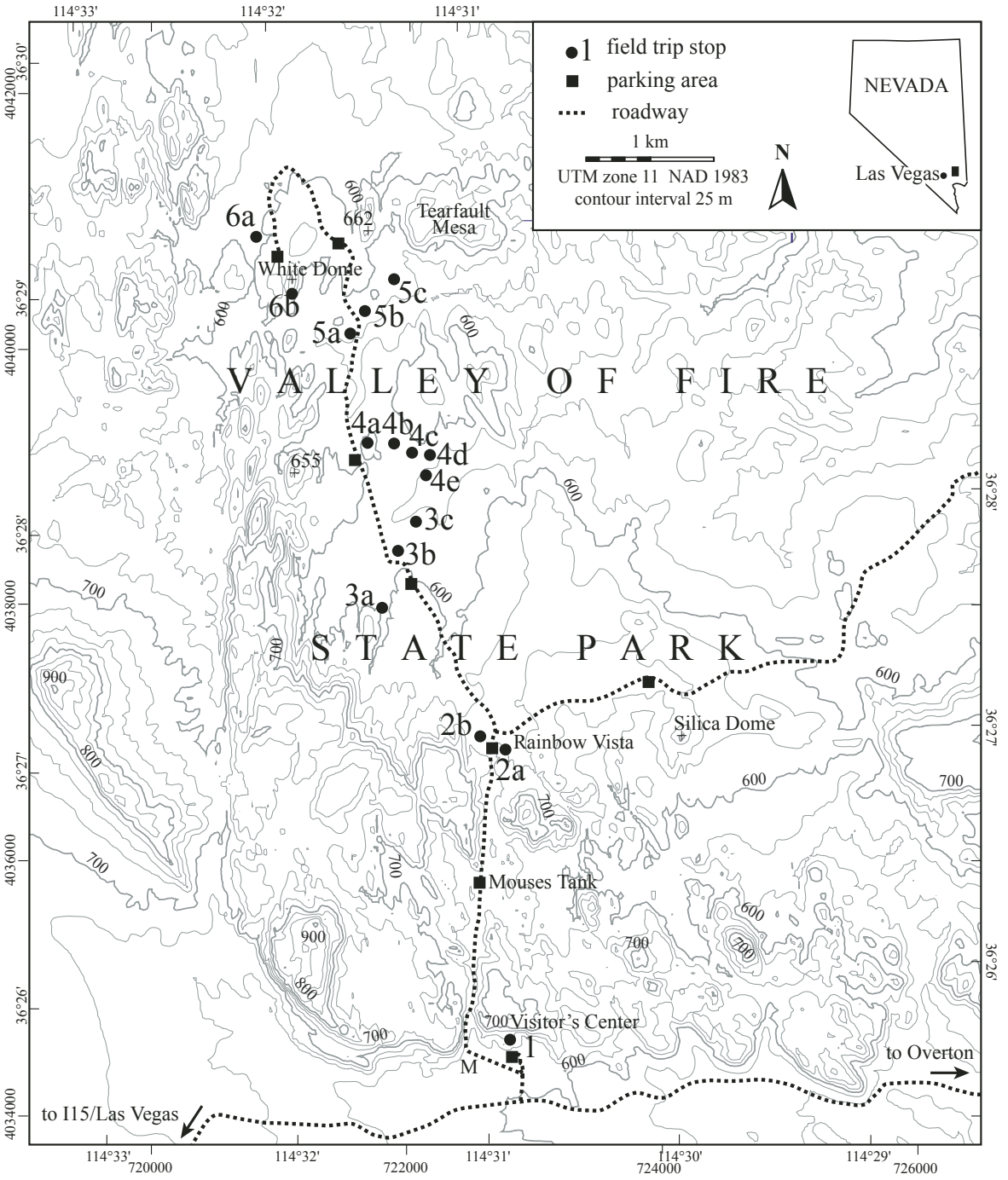

Figure 6. Map of field trip stops in Valley of Fire State Park; same area as Figure 2.

is uniform without regard to grain size variations among cross-stratified layers. Immediately to the north of the Rainbow Vista parking area, the color changes to yellow and purple over a relatively sharp 1–5-cm-wide boundary. This color boundary is offset along the Mouses Tank fault by 150 m of left-lateral slip. The boundary is parallel to bedding over distances of 10–100 m but frequently climbs, and occasionally drops, across bedding over distances of 10–50 m. This color boundary is thus diagenetic and not depositional in origin. This and other similar color boundaries will thus be referred to as alteration contact. In the Rainbow Vista area, the average orientation of the alteration contact dips to the northeast by up to 49° compared to bedding at 22°. The uni-

formly red sandstone in the lower part of the Aztec Sandstone is referred to as "lower red unit" in Figures 2 and 3, and the yellow and purple alteration forms part of the middle alteration units.

The alteration contact has a lobate-cuspate geometry, shown schematically in Figure 4, with lobes of purple or yellow sandstone penetrating the lower red sandstone. One such lobe is visible on the cliff facing Rainbow Vista, west of the road. We interpret this lobate-cuspate alteration contact as a reaction boundary that migrated into the red sandstone, changing the red to yellow. This interpretation is consistent with a syndepositional origin of the hematite grain coat in uniformly red sandstone. The structural offset of this alteration contact along the Mouses Tank fault indicates that this bleaching occurred prior to slip on the Mouses Tank fault, or at least prior to the last 150 m of slip along this fault. We will see evidence at subsequent stops that the syndepositional reddening of the Aztec Sandstone and the yellow and purple alteration are separated by an intermediate alteration stage characterized by banded orange-and-white rock colors. This second stage of alteration has been completely overprinted at Rainbow Vista by the third stage of yellow and purple alteration.

A flat exposure of Aztec Sandstone ~20 m east of the parking area exhibits cross-cutting relations among compaction bands, shear bands, joints, and sheared joints. Subvertical, NNW-SSE–striking, 1–2-cm-thick compaction bands are the oldest structures. They are offset by ~1 cm of slip along subhorizontal shear bands and accompanying slip surfaces that follow depositional surfaces. Slip along these shear bands is top to the south. Joints follow earlier compaction and shear bands. The youngest discernible stage of deformation is slip along these joints, resulting in the formation of tail cracks at a high angle to the sheared joints.

Where compaction bands cross the alteration contact between lower red and middle yellow and purple sandstone, the alteration contact appears in some instances offset along the bands even where depositional surfaces are not offset. These offsets of the alteration contacts are interpreted to reflect the retardation of the moving reaction boundary across the lower-permeability compaction band. Examples are visible on the cliffs to the east of Rainbow Vista. We will discuss this effect again at Stop 6a.

Cross the park road and walk 60 m W to exposures of the N-S–striking Mouses Tank fault.

Stop 2b—Mouses Tank Fault as a Joint-Based Fault

This stop provides the first example of a fault zone that formed by shearing along preexisting joint zones. This zone has at least 150 m of net left-lateral strike-slip and is structurally quite complex (Fig. 7A). The 0.5–1-m-thick fault core is composed of fault rock and slip surfaces, the latter with an overall orientation parallel to the fault strike. The 2–3-m-thick fault damage zone is composed of joints, sheared joints, and deformation bands. Joints are frequently oriented at an oblique angle to sheared joints, with a characteristic splay fracture geometry.

Following Myers (1999) and Flodin and Aydin (2004), the evolution of these faults includes the formation of joints, slip along joints, formation of splay or tail fractures, and linkage of sheared joints. Structural elements that comprise joint-based faults include joints, sheared joints, shear bands, fragmented rock, fault rock, and slip surfaces. Four end-members of preexisting joint zone geometries are recognized (Myers and Aydin, 2004; Flodin and Aydin, 2004): (1) en-échelon joint zones that have step-sense opposite to shear-sense (e.g., right-stepping and left-lateral shearing); (2) en-échelon joint zones that have step-sense similar to shear-sense (e.g., right-stepping and right-lateral shearing); (3) subparallel joint zones characterized by a large joint-length to joint-spacing ratio; and (4) individual joints with attendant fringe joints (or hackle). For en-échelon joint zones that have a step-sense opposite to the slip-sense, the overlapping region between stepping joints is subject to a localized contractional strain (Segall and Pollard, 1980; Lin and Logan, 1991), which results in the frictional breakdown of host rock material. Damage in the form of joints and sheared joints is outwardly developed (Myers, 1999). In contrast, en-échelon joint zones that have the same step-sense and slip-sense are subject to a localized dilational strain that results in the fragmentation of rock that spans the overlapping en-échelon joints by inwardly directed splay fractures. For subparallel joint zones, strain is accommodated by the formation of splay fractures that span the distance between the overlapping joint segments. Accumulated shear strain is preferentially localized along the closely-spaced subparallel sheared joints (Myers and Aydin, 2004).

This stop also illustrates large-scale permeability effects of the fault zones. From a hydrologic perspective, the joint-based faults in the Valley of Fire are composed of high permeability components (joints, splay fractures, and slip surfaces) and low permeability components (fault rock, deformation bands, and sheared joints) embedded in a matrix with intermediate permeability. Using a detailed map of a portion of Mouses Tank fault drafted by Myers (1999), Jourde et al. (2002) derived bulk permeability values for this fault zone using numerical upscaling methods (Fig. 7). The upscaling work flow starts with subcentimeter-resolution field maps that distinguish the various elements of the fault zone (Fig. 7A). The permeability values of each fine scale fault zone element (joints, sheared joints, fault related deformation bands, slip surfaces, fault rock, and the matrix rock) are either measured or estimated (Fig. 7B) and then input into the detailed description (Fig. 7C). Numerical simulation of the fine-scale input map yields the larger-scale permeability of the fault zone of interest (Fig. 7D).

For both map regions featured in Figure 7, the fault-perpendicular component of permeability (k_1) is reduced by over two orders of magnitude relative to the host rock. This large reduction is clearly due to the wide zone of fault rock and to the fact that there are no slip surfaces traversing this zone in the perpendicular direction. The dense regions of deformation bands at stepovers and sheared joints emanating out from the gouge also contribute

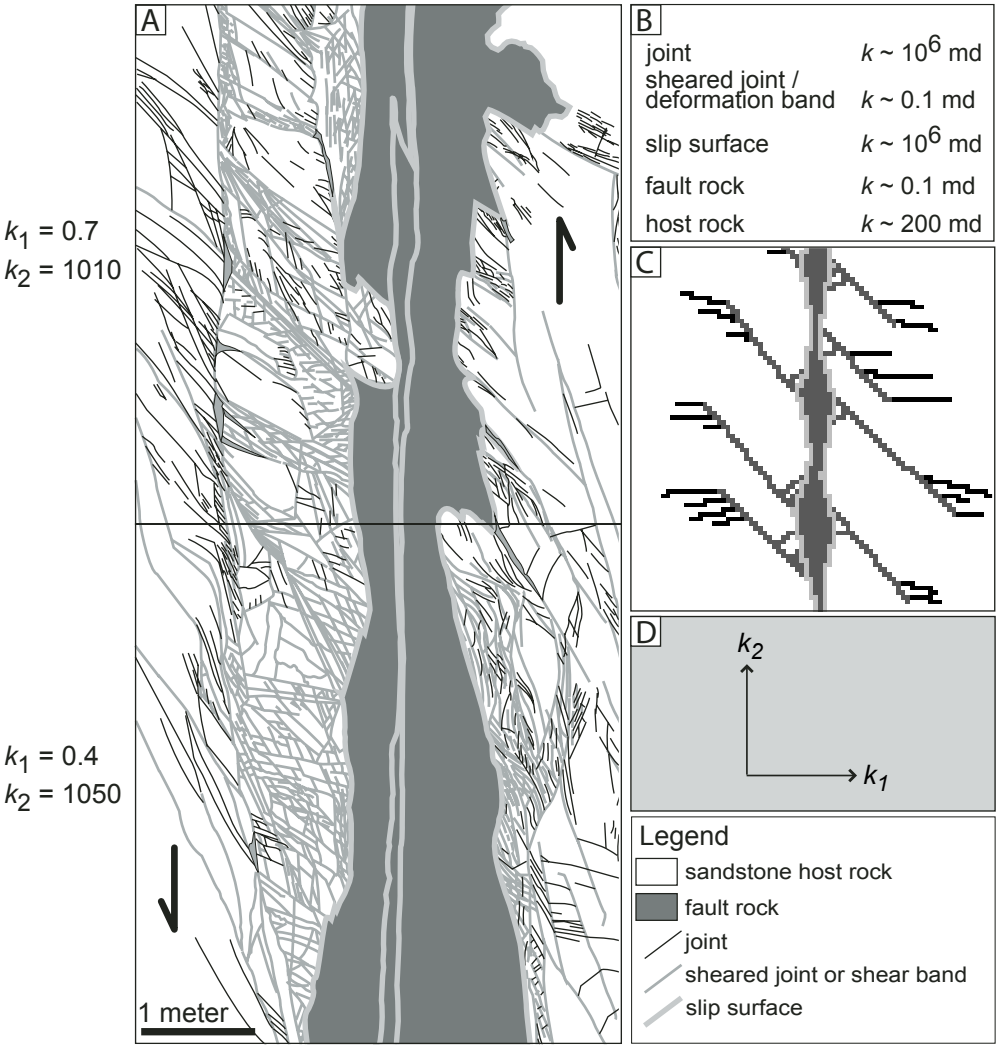

Figure 7. Workflow used to upscale fault zone permeability. (A) Map of Mouses Tank fault with 150 m of strike-slip, from Myers (1999). Values of large-scale permeability k_1 and k_2 (in md) as calculated by Jourde et al. (2002) for each map area as computed in step (D). (B) Laboratory analysis for fault element permeability. (C) Rasterization of field map and assignment of element permeability values. (D) Numerical calculation of large-scale permeability.

to the low fault-normal permeability. The continuous slip surfaces in the direction along the fault lead to enhanced permeability in the fault-parallel direction.

Directions to Stop 3

Follow the park road north toward White Dome for 1 mile (1.6 km) and park at the next parking area (parking area 1) to the left of the road. Walk ~120 m west to a prominent south-facing fault exposure.

Stop 3a—Structure, Petrophysics, and Permeability of a Joint-Based Fault with ~25 m Slip

This location provides a well-exposed cross section across the Lonewolf fault with ~25 m of left-lateral strike-slip (Fig. 2) and associated secondary and higher order structures. This exposure was one of three sampling stations in a study of fault rock petrophysics (Flodin et al., 2005). Four basic rock elements are identified (Fig. 8): (1) undamaged host rock; (2) damaged host rock; (3) fragmented rock; and (4) fault rock. No bulk mineralogical changes due to fault zone cementation or mineral alteration are detected when comparing host and fault rock. Fault rock permeability is one to three orders of magnitude lower than median host rock permeability. Porosity reductions are less pronounced and show considerable overlap in values between the sample suites. Some fragmented rock samples appear to have dilated with respect to median host rock porosity. Median grain sizes for fault rock samples range from 3 to 51 μm, which is up to two orders of magnitude reduction from host rock median grain sizes. There appears to be a lower limit of median grain size of 3 μm for fault rock samples irrespective of average fault shear strain. Fault rock capillary injection pressures range from one to almost two orders of magnitude higher than host rock equivalent. Based on these measurements, we conclude that faults formed by shearing of

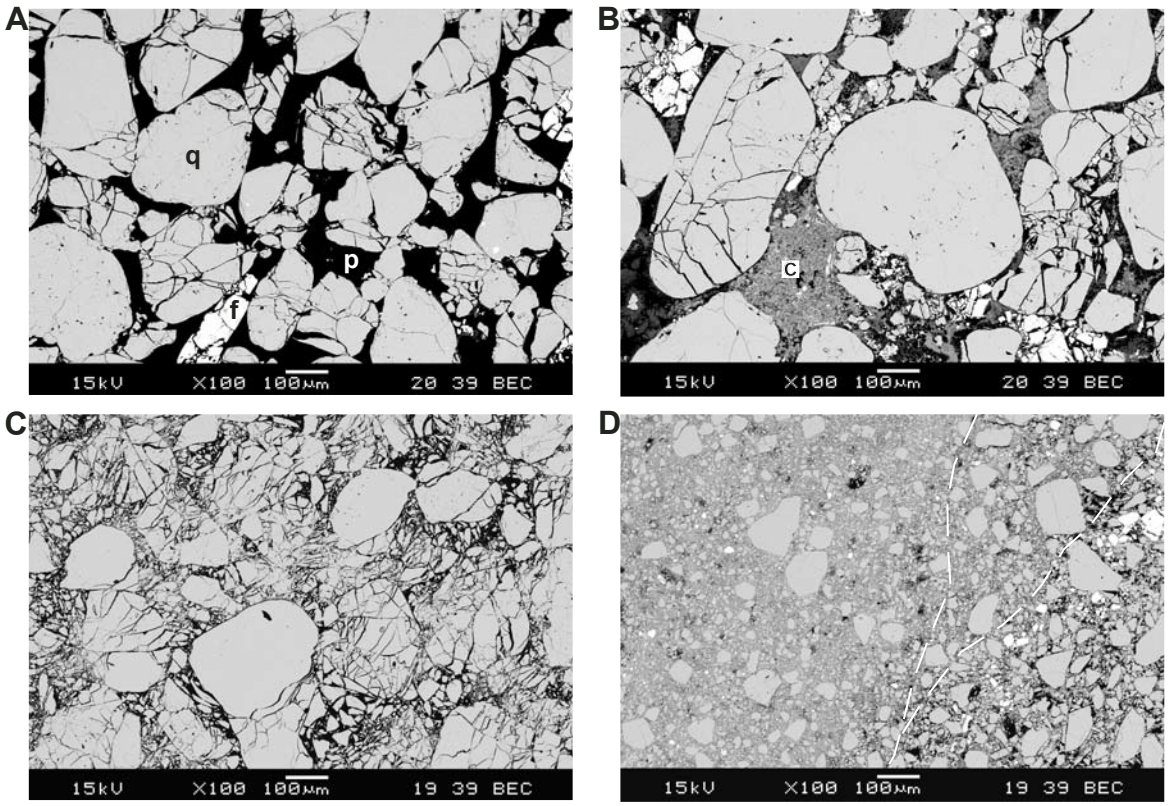

Figure 8. Backscatter electron images of deformed Aztec Sandstone at Stop 3a. White minerals are potassium feldspar; light gray minerals are quartz; dark gray minerals are clays; black is pore space. (A) Host rock fragment showing earliest signs of grain-scale fragmentation. Nearly every grain shows varying degrees of fracturing; however, the primary pore space is preserved. f—potassium feldspar, p—pore space, q—quartz. (B) Host rock collected adjacent to fault core. Note that many of the grains are fractured and that much of the pore space is occupied by clay minerals (c). (C) Host rock collected adjacent to the fault core showing signs of severe grain-scale fragmentation, collapse of pores, and low primary porosity. (D) Well-developed fault rock characterized by severe grain size reduction and a complete loss of primary porosity. Dashed lines are approximate locations of slip surfaces. Note the variability with respect to pore space (black) between the left and right sides of the image. Figure adapted from Flodin et al. (2005).

joints in high permeability sandstone systems will act as significant barriers to fluid flow on short time scales and might be capable of sealing small to moderate hydrocarbon columns on a geologic time scale as well, assuming adequate continuity of the fault rock over large areas of the fault.

Follow the fault NNE across the park road. Walk E along the far side of the park road for ~20 m, then veer to the NW at the first small valley and walk ~5 m.

Stop 3b—Small-Scale Material Rotation

Material rotations play an important role in the conceptual framework for the development of the fault system in the Valley of Fire. Importantly, material rotations allow for newly resolved shear stresses across fractures that originated as opening-mode joints. At this stop we see evidence for small-scale material rotation in the vicinity of a fault zone. This example is from a left stepover between right-lateral bounding faults that show cumulative separations on the order of a few meters. Traversing the stepover area are a set of left-lateral faults and two steeply dipping, preexisting deformation bands that enter the fault zone from the northeast. Outside of the fault zone, both deformation bands continue with a straight trace for many meters toward the northwest. Within the fault zone, the deformation bands are broken and offset by left-lateral faults that are bound between the two overlapping right-lateral faults. Between the left-lateral faults, the deformation band segments approximately retain their straight trace. The deformation band segments are progressively rotated in a clockwise sense with increasing distance to the lower right-lateral fault. At the last documented juncture between the deformation bands and the right-lateral fault, the bands are rotated by as much as 60°. A best-fit great circle through the orientation data indicates the deformation bands were rotated about axes that plunge ~70°.

Follow the main trace of the Lonewolf fault zone 220 m to the NNE.

Stop 3c—Fault Hierarchies and Network Evolution

Mutual abutting relationships between different sets of left- and right-lateral faults and splay fractures at this locality imply a hierarchical sequence of formation. Here, the largest structure is the left-lateral Lonewolf fault. We consider the Lonewolf fault primary in nature because it bounds all other structures. Emanating from the Lonewolf fault are splay fractures and right-lateral faults that share the same orientation. These structures are considered to be second generation because they appear to have formed in response to activity along the primary Lonewolf fault. All secondary structures have at least one end that abuts against a primary left-lateral fault. Two of the second-generation right-lateral faults extend through the map area to the southwest where they join with the end of the Classic fault to the southwest. Emanating from, and localized between, these two right-lateral faults are splay fractures and left-lateral faults, both of which have the same intersection angle. These structures are considered to be third-generation because they appear to be genetically related to activity along the second-generation structures. All third-generation structures are bound on at least one end by a second generation right-lateral fault. Further branching occurs from the third-generation left-lateral faults in the form of fourth-generation splay fractures, the subsequent shearing of which produced a fourth-generation of right-lateral faults. The highest order structure identified in this area is a fifth-generation left-lateral fault and related splay fractures.

In the conceptual model shown in Figure 9, the first generation of faults with a left-lateral sense of shearing produces opening-mode splay fractures that are primarily localized at or near the end, and in the immediate vicinity, of the first-generation structures. However, due to mechanical interaction between adjacent first-generation faults (Martel, 1990) and in response to increasing slip, some splay fractures propagate across the distance of undeformed rock that spans these neighboring structures (Fig. 9). Due to local stress perturbations between overlapping faults (e.g., Segall and Pollard, 1980; Kattenhorn et al., 2000; Bourne and Willemse, 2001; Peacock, 2001) and material rotations (e.g., Nur et al., 1986; Nicholson et al., 1986), shear stress is imposed across the first-generation splay fractures to form second-generation faults (right-lateral) with their associated second generation splay fractures (Fig. 9). These second-generation splay fractures, like the first-generation splay fractures, form locally between fault stepovers and outwardly from fault ends. The second generation faults almost always have a slip sense opposite to that of the first generation faults formed earlier (Fig. 9).

An exception to the rule of consistent orientation and sense of slip is illustrated where an earlier splay fracture emanating from a primary left-lateral fault is more optimally oriented for the imposition of left-lateral shear (upper right, Fig. 9) and thus forms a left-lateral fault in a rather uncommon orientation. Splay fractures formed from right sense of slip across the second-generation faults are oriented subparallel to the first-generation left-lateral faults. This process is repeated to form successively younger generations of faults and splay fractures as slip accumulates along, and transfers between, the first generation faults (Fig. 9). The final fault network geometry is defined by the order and characteristic kink angle of splay fractures. Deviations that occur for intersection angles between faults and splay fractures might stem from the presence of complex preexisting joint geom-

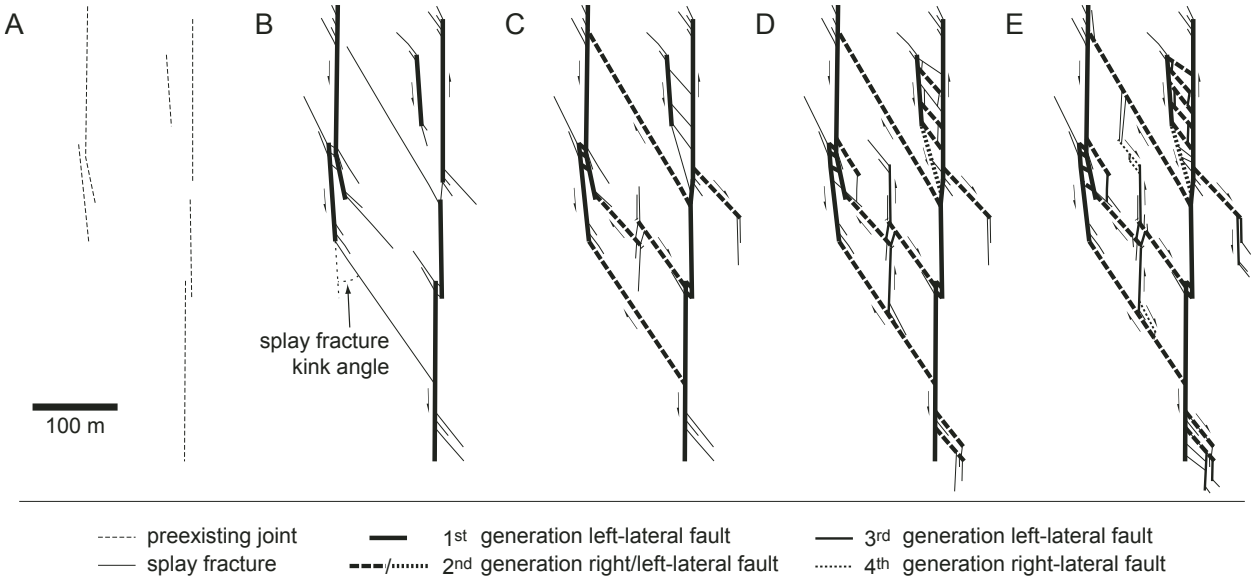

Figure 9. Conceptual model for the evolution of the strike-slip fault network at Valley of Fire. (A) Preexisting joints prior to, or at the earliest phase of, faulting. (B–E) Progressive stages of splay fractures that evolve into hierarchical sets of left- and right-lateral faults. Figure adapted from Flodin and Aydin (2004).

etries, the formation of splay fractures at lower angles between left- and right-lateral faults, and/or material rotations.

Directions to Stop 4

Follow the park road 0.6 mi (1 km) to the next parking area (no. 2) to the left of the road. Park your vehicle, cross to the east-side of the road, and climb atop the hills 180 m N of the parking area.

Stop 4a—Upper Aztec Sandstone Alteration Overlook

Looking north, this vantage point provides a cross-sectional view across the upper alteration units of the Aztec Sandstone (Fig. 3). Yellow and banded orange-and-white alteration colors are visible in the foreground. A layered sequence of purple, yellow, orange, white, and red colors forms the uppermost part of the section in the background. Red sandstone forms the top of White Dome to the NNW. This uniform red sandstone alteration is similar to the lower red alteration unit in the lower part of the Aztec Sandstone and is thus designated as upper red alteration. The layered alteration sequence is, at first approximation, parallel to bedding, which dips to the right (ENE). In the far background to the north, Tearfault Mesa forms a klippe of the Willow Tank thrust sheet. A closer look at the thrust and associated alteration is provided at Stop 5c.

Within the regional cross section (Fig. 4), the yellow colors in the foreground are part of a roughly symmetric alteration pattern with yellow and banded orange-and-white units in the center, overlain and underlain by purple and yellow and the red sandstone of the upper and lower red units. The symmetry is broken by the occurrence of white and orange bands along the boundary to the upper red unit, and by the banded red-and-white sandstone above the upper red unit, visible between White Dome and the park road to the east. The central occurrence of yellow and purple sandstone forms a lobe that occupies most of the middle alteration units to the southeast and tapers off to the northwest. Although the alteration units are orientated roughly parallel to bedding, the top boundary of this lobe is less inclined than the other alteration bands, allowing the overlying banded orange-and-white unit to increase in thickness toward the northwest (Fig. 4).

The orientation of the alteration units roughly parallel to the stratigraphic sequence suggests that the flow of fluids causing this alteration was to a large extent controlled by stratigraphic boundaries and bedding (Fig. 5). The Aztec Sandstone is overlain by mudstone of the Willow Tank Formation, which likely acted as an aquitard or seal for the permeable Aztec Sandstone aquifer. In addition, the regional scale distribution of alteration and fluid flow was affected by faults, as seen at closer range at Stop 5b.

Walk east 270 m across a sand-covered area to the next exposure of banded orange-and-white sandstone. Notice deformation bands forming vertical fins on bare rock surfaces due to the higher erosion resistance of deformation bands relative to the surrounding sandstone.

Stop 4b—Effect of Deformation Bands on Alteration and Fluid Flow

This stop illustrates the interplay of depositional and structural heterogeneities on alteration and fluid flow on the outcrop scale. The banded orange-and-white alteration unit is characterized by an orange stain in the finer-grained sedimentary layers and the absence of pigment in the coarser-grained layers. This banding results in an alternating sequence of ~10–20-cm-thick orange and white layers that follow depositional bedding. In addition to this depositional control, the distribution of pigment is affected by deformation bands that act as boundaries that separate compartments with internal color gradients from orange to white. The effect of deformation bands on the distribution of the orange stain reflects the lower permeability of deformation bands relative to the more permeable surrounding sandstone. Following Antonellini and Aydin (1994) and Sigda et al. (1999), the permeability of deformation bands is typically 2–3 orders of magnitude lower compared to the adjacent sandstone. Deformation bands thus form baffles to the movement of pore fluid across otherwise more permeable sandstone.

The distribution of pigment in banded orange-and-white sandstone may thus give a visual cue to the permeability structure of the sandstone, being controlled by both depositional layering and deformation bands. Assuming that the sandstone is reddened preferentially on the upstream side of deformation bands, Eichhubl et al. (2004) inferred a NE- and downward-directed flow direction for this location. A SW- and upward-directed flow direction was obtained at a location 1.5 km to the NW. They concluded that the alteration pattern provides consistent flow directions on the outcrop scale but varies on the regional scale.

Walk 180 m SE to a N-S–trending gully. The east side of the gully exposes the contact of banded orange-and-white alteration at the base against yellow and purple sandstone at the top.

Stop 4c—Crosscutting Relations of Second and Third Alteration Stages

The contact between banded orange-and-white and yellow and purple alteration provides a relative age constraint on the timing of alteration and, by association, of fluid flow. The yellow and purple alteration cuts across the banded orange-and-white alteration, suggesting that the banded orange-and-white alteration predates the yellow and purple alteration. In addition, the banded orange-and-white alteration is altered to purple-and-white along this contact, also suggesting that the yellow and purple alteration postdates the banded orange-and-white alteration. We interpret this alteration pattern to be the result of dissolution and reprecipitation of iron oxide and hydroxide cement. Increasing steps of dissolution and reprecipitation lead to a coarsening of iron oxide and hydroxide, with a resulting change in color from red and orange to yellow and purple. We attribute the banded orange-and-white stain to a second stage of alteration, distinct from a third stage of alteration that resulted in yellow and purple alteration.

The three alteration stages at Valley of Fire therefore include (1) a syndepositional stage resulting in the uniform red stain of the lower and upper red alteration units; (2) a second stage of alteration resulting in banded orange-and-white alteration; and (3) a third stage characterized by yellow and purple colors (Fig. 5).

Walk 50 m to a deep N-S–trending canyon. This canyon follows one branch of the Lonewolf fault we examined farther south at Stops 3a–3c. A second branch of the fault is in the parallel canyon 20 m east.

Stop 4d—Segmented Faults and Meso-Scale Material Rotation

The Lonewolf fault offsets the lower contact of the upper red sandstone by 33 m of left-lateral slip. Similar to the upper contact of the lower red sandstone, this alteration contact predates fault slip along these high-angle faults.

Here, we see another example of material rotation between segmented strike-slip faults, though larger in scale and opposite in rotation sense compared to Stop 3b. In this case, the bounding faults are left-lateral and the internal faults are right-lateral. The bounding faults are the right-stepping northern and central segments of the Lonewolf fault. The internal right-lateral faults intersect their bounding faults at angles ranging from 27° to 60°. Oriented perpendicular to, and offset by, the two segments of the left-lateral Lonewolf fault is a zone of earlier-formed deformation bands. The zone of deformation bands itself consists of bounding deformation bands that show right-lateral separation and internal deformation bands that show left-lateral separation and are similar in geometry to zones of deformation bands described by Davis et al. (2000). The mean angle of intersection between the two deformation band sets is ~26° both inside and outside of the bounding segments of the Lonewolf fault. However, mean orientations of the two sets that occur between the fault segments are rotated ~15° in a counterclockwise sense with respect to the zones of deformation bands found outside of these segments. Some of the internal right-lateral faults appear to be rotated as well.

Walk 180 m south along the trace of the Lonewolf fault, to the south end of the canyon.

Stop 4e—A Fault Core with ~25 m Slip and Low Average Shear Strain

At this stop, we will visit another outcrop of the Lonewolf fault core. As at Stop 3a, the Lonewolf fault at this locality has ~25 m of left-lateral slip. However, the fault core here is much wider than the core at Stop 3a, resulting in a lower value of average shear strain across the zone. The lower shear strain appears to have an impact on fault rock petrophysics. Of the three sampling stations, this locality exhibits the least amount of permeability reduction.

Unlike the lower contact of the upper red sandstone, which is offset 33 m along this fault, purple bands at this location cross the fault with minimal, if any, mechanical offset. We conclude that the purple and, by association, yellow alteration largely postdates faulting along these high-angle faults of inferred Tertiary age.

Directions to Stop 5

Return to the vehicles. Follow the park road north 1.1 mi (1.8 km) and park at parking area 3. Walk back along the road 830 m; Stop 5a is 10 m to the west of, and below, the road, ~130 m north of Kaolin Wash.

Stop 5a—Preferred Fluid Flow and Alteration along Sheared Joints

Following the road back from parking area 3, we crossed from upper red Aztec Sandstone through some white alteration into a 10–20-m-thick band of orange sandstone (Fig. 3). We also note that the alteration colors do not appear to continue across the road with orange sandstone on the west side against yellow and purple sandstone on the east side. This mismatch is due to slip along the N-S–striking Bighorn fault. This fault, which follows the road from the last turn onward, offsets the orange, white, and red alteration units by 600–700 m of apparent left-lateral strike-slip. A purple band ~30 m south of the yellow to orange contact also appears offset along the fault but only by 10–20 m. An exact amount is difficult to determine due to the presence of the road. In accordance with our finding at the Lonewolf fault, we can conclude, however, that the yellow and purple alteration formed later than the orange, white, and upper red alteration units—the former during late stages of faulting, the latter prior to faulting.

Joints across the lower contact of the orange alteration zone and extending into the underlying white sandstone are characterized by orange alteration halos. In some instances, the lower boundary of the orange alteration zone is deflected downward along these joints as elongate orange lobes, consistent with these joints acting as preferred conduits for fluid flow and mass transfer. The preferred staining along these joints also indicates that the orange stain is secondary to the bleaching of the white sandstone. Following the observation that the orange alteration unit is offset by the same amount as the white and upper red contacts, and thus predated fault slip, we interpret the orange halos around these joints as a secondary remobilization of the orange stain after faulting initiated. These alteration halos are in part offset by 1–3 cm of left-lateral slip, kinematically compatible with slip along the Bighorn fault and thus interpreted as coeval with fault movement.

Follow the Bighorn fault back north, up the hill along the road. Where the road swings northwest, leave the road and continue straight along the fault for 160 m.

Stop 5b—Influence of Bighorn Fault on Alteration and Fluid Flow

Following the Bighorn fault northward, the fault separates red and banded red-and-white sandstone to the west (left) from

yellow and purple sandstone to the east. Walking up the hill, we observe purple and orange alteration bands on the east side of the fault changing orientation adjacent to the fault, turning from an orientation roughly parallel to bedding into parallelism upon approaching the fault. This indicates that the reactions leading to the formation of these bands were affected by the presence of the Bighorn fault, thus dating these reactions to after, or concurrent with, the formation of the fault. Unlike the mechanical fault offset observed for contacts of the lower and upper red sandstone and for banded orange-and-white sandstone, this deflection of the purple and orange bands is not due to shearing along the fault. Instead, we interpret this deflection to be the result of remobilization and "bleeding" of iron across the fault where the fault juxtaposes red sandstone against bleached sandstone. A similar deflection of purple and yellow bands is observed along faults south of Kaolin Wash and along the Classic fault.

Continue along the Bighorn fault. Upon approaching a gravel-capped low hill to the left, turn east for ~300 m to obtain a good view of Tearfault Mesa to the north and of the alteration of the underlying Aztec Formation.

Stop 5c—Tearfault Mesa Overlook: Effect of Thrusting on Alteration and Fluid Flow

Tearfault Mesa is a tectonic klippe of allochthonous Aztec Sandstone, resting on gravel, sandstone, and gray mudstone of the Cretaceous Willow Tank Formation. The Willow Tank Formation, in turn, overlies in depositional contact the Aztec Sandstone that forms the bulk of Aztec exposure in the park (Figs. 3 and 4). This klippe is part of the Willow Tank thrust sheet, the lowermost and easternmost Sevier thrust sheet in this area (Longwell, 1949; Bohannon, 1983). Along the eastern tip of Tearfault Mesa, the beds of the Willow Tank Formation are locally overturned, reflecting the eastward movement of the thrust front. An E-W–striking tear fault, which is difficult to discern from this vantage point, forms the southern boundary of the klippe. The Bighorn fault cuts across and offsets vertically the Willow Tank thrust sheet, consistent with a Tertiary age of the Bighorn fault.

The upper red alteration of the Aztec Sandstone is bleached white in the vicinity of the thrust. This suggests that (1) the uniform red color of the upper red sandstone, considered the first alteration stage, predates the thrusting; and (2) that bleaching of the upper red is synchronous to or postdates thrusting. A pre-thrust age of red alteration of the Aztec Sandstone was also deduced by Longwell (1949) based on the ubiquitous occurrence of red Aztec clasts in the Willow Tank Formation. Although no direct cross-cutting relations are observed between the bleaching on top of the upper red alteration unit with the other alteration units, we correlate this bleaching with the fluid flow event that caused the banded orange-and-white alteration at stratigraphically and structurally deeper levels. These alteration stages are mechanically offset by the high-angle faults of Tertiary age, thus predating these faults.

Directions to Stop 6

Return to vehicles and follow the park road to its end at the White Dome parking area. Walk back along the road for 200 m, then turn left (W), following a marked trail for 100 m.

Stop 6a—Deformation Bands as Flow Barriers

The south- to west-facing rock exposure contains the lower contact of the orange alteration unit observed farther east at Stop 5a. At this location, this alteration contact appears offset along deformation bands by 15–20 cm. Taylor and Pollard (2000) noted that these offsets are not due to slip along these bands, which rarely exceeds a few millimeters. Rather, these offsets are due to the retardation of a reaction boundary across these bands relative to the undeformed sandstone. Taylor and Pollard (2000) attributed this retardation to the reduced permeability of these bands. Assuming that these bands would retard the velocity of a sweeping reaction boundary to the same degree as the fluid flow velocity, they calculated a reduction in permeability across these bands by one to two orders of magnitude. This estimate is approximately one to two orders of magnitude lower than measurements by Antonellini and Aydin (1994) for deformation bands in similar eolian sandstone. We note that the velocity of a moving reaction boundary would, in fact, be slower than the flow velocity of the reacting aqueous solution. The calculated permeability reduction is thus a minimum estimate of the actual permeability reduction, which could account for the difference from the measured values by Antonellini and Aydin (1994).

Return to the parking area and walk along the marked hiking trail to the south of the parking area through the wind gap west of White Dome. Where the trail drops into the drainage to the south, leave the trail and follow the sandstone ledges to your left, gaining some height, to the ridge south of White Dome. Use caution walking on the slick rock surfaces!

Stop 6b—Summary Overlook of Valley of Fire Alteration and Fluid Flow

This vantage point provides a sweeping view over the northern part of Valley of Fire, with the tectonic klippe of Tearfault Mesa to the east and Silica Dome, marking the contact of lower red to middle alteration units, to the far southeast. We are standing on yellow and purple alteration that cuts across banded orange-and-white alteration. Yellow and purple alteration is overlain by orange and white alteration units, and, close to the top of White Dome, a bit of upper red. The alteration units are overall parallel or subparallel to bedding, which dips NE at 20°.

This view summarizes well the complex interaction of diagenetic alteration and fluid flow with depositional and structural heterogeneities in the Aztec Sandstone at Valley of Fire: On the outcrop scale, alteration and fluid flow are influenced and controlled by bedding, deformation bands, and joints. On the regional scale, alteration and fluid flow are controlled by

formation contacts and large scale structures, including the Willow Tank thrust, with Tearfault Mesa as its erosional remnant. Although the depositional, structural, hydrogeologic, and diagenetic history is challenging to decipher, Valley of Fire provides a perhaps unique, and certainly picturesque, view into the complex interaction among these processes in the subsurface.

Return along the trail to the White Dome parking area. Return to Las Vegas.

ACKNOWLEDGMENTS

We thank A. Aydin and D.D. Pollard, Stanford University, for introducing us to Valley of Fire geology, promoting this research, and for sharing their ideas. Material presented here includes work performed by former Stanford students and postdocs including J. Chapin, H. Jourde, R. Myers, K. Sternlof, and W.L. Taylor. This research was funded by U.S. Department of Energy grant DE-FG 03-94ER14462, with additional funding from the Stanford Rock Fracture Project (RFP) industrial affiliate program, Chevron Energy Technology Company, and Stanford University.

REFERENCES CITED

Anderson, R.E., and Barnhard, T.P., 1993, Heterogeneous Neogene strain and its bearing on horizontal extension and horizontal and vertical contraction at the margin of the extensional orogen, Mormon Mountains area, Nevada and Utah: U.S. Geological Survey Bulletin, B2011, 5 sheets, 113 p.

Antonellini, M.A., and Aydin, A., 1994, Effects of faulting on fluid flow in porous sandstones: petrophysical properties: AAPG Bulletin, v. 78, p. 355–377.

Axen, G.J., 1993, Ramp-flat detachment faulting and low-angle normal reactivation of the Tule Springs thrust, southern Nevada: Geological Society of America Bulletin, v. 105, p. 1076–1090, doi: 10.1130/0016-7606(1993)105<1076:RFDFAL>2.3.CO;2.

Aydin, A., 2000, Fractures, faults, and hydrocarbon migration and flow: Marine and Petroleum Geology, v. 17, p. 797–814, doi: 10.1016/S0264-8172(00)00020-9.

Blakey, R.C., 1989, Triassic and Jurassic geology of the southern Colorado Plateau, *in* Jenny, J.P., and Reynolds, S.J., eds., Geologic evolution of Arizona: Arizona Geological Society Digest, v. 17, p. 369–396.

Bohannon, R.G., 1977, Geologic map and sections of the Valley of Fire region, North Muddy Mountains, Clark County, Nevada: U.S. Geological Survey Miscellaneous Field Studies Map MF-849, scale 1:25,000.

Bohannon, R.G., 1983, Mesozoic and Cenozoic tectonic development of the Muddy, North Muddy, and northern Black Mountains, Clark County, Nevada: Geological Society of America Memoir 157, p. 125–148.

Bohannon, R.G., 1992, Geologic map of the Weiser Ridge quadrangle, Clark County, Nevada: U.S. Geological Survey Report GQ-1714, 1 sheet, scale 1:24,000.

Bohannon, R.G., Grow, J.A., Miller, J.J., and Blank, R.H., Jr., 1993, Seismic stratigraphy and tectonic development of Virgin River depression and associated basins, southeastern Nevada and northwestern Arizona: Geological Society of America Bulletin, v. 105, p. 501–520, doi: 10.1130/0016-7606(1993)105<0501:SSATDO>2.3.CO;2.

Bourne, S.J., and Willemse, E.J.M., 2001, Elastic stress control on the pattern of tensile fracturing around a small fault network at Nash Point, UK: Journal of Structural Geology, v. 23, p. 1753–1770, doi: 10.1016/S0191-8141(01)00027-X.

Caine, J.S., Evans, J.P., and Forster, C.B., 1996, Fault zone architecture and permeability structure: Geology, v. 24, p. 1025–1028, doi: 10.1130/0091-7613(1996)024<1025:FZAAPS>2.3.CO;2.

Carpenter, D.G., 1989, Geology of the North Muddy Mountains, Clark County Nevada, and regional structural synthesis: fold-thrust and Basin-Range structure in southern Nevada, southwest Utah and northwest Arizona [M.S. thesis]: Corvallis, Oregon State University, 145 p.

Carpenter, D.G., and Carpenter, J.A., 1994, Fold-thrust structure, synorogenic rocks, and structural analysis of the North Muddy and Muddy Mountains, Clark County, Nevada, *in* Dobbs, S.W., and Taylor, W.J., eds., Structural and stratigraphic investigations and petroleum potential of Nevada, with special emphasis south of the Railroad Valley Producing Trend: Nevada Petroleum Society 1994 Conference Volume II: Reno, Nevada, Nevada Petroleum Society, p. 65–94.

Davis, G.H., Bump, A.P., Garcia, P.E., and Ahlgren, S.G., 2000, Conjugate Riedel deformation band shear zones: Journal of Structural Geology, v. 22, p. 169–190, doi: 10.1016/S0191-8141(99)00140-6.

Dickinson, W.W., and Milliken, K.L., 1995, The diagenetic role of brittle deformation in compaction and pressure solution, Etjo Sandstone, Namibia: Journal of Geology, v. 103, p. 339–347.

Eichhubl, P., and Behl, R.J., 1998, Diagenesis, deformation, and fluid flow in the Miocene Monterey Formation of coastal California, *in* Eichhubl, P., ed., Diagenesis, deformation, and fluid flow in the Miocene Monterey Formation of coastal California: Society for Sedimentary Geology (SEPM) Pacific Section Special Publication 83, p. 5–13.

Eichhubl, P., and Boles, J.R., 2000, Focused fluid flow along faults in the Monterey Formation, coastal California: Geological Society of America Bulletin, v. 112, p. 1667–1679, doi: 10.1130/0016-7606(2000)112<1667:FFFAFI>2.0.CO;2.

Eichhubl, P., Taylor, W.L., Pollard, D.D., and Aydin, A., 2004, Paleofluid flow and deformation in the Aztec Sandstone at the Valley of Fire, Nevada—Evidence for the coupling of hydrogeologic, diagenetic, and tectonic processes: Geological Society of America Bulletin, v. 116, p. 1120–1136, doi: 10.1130/B25446.1.

Flodin, E.A., and Aydin, A., 2004, Evolution of a strike-slip fault network, Valley of Fire State Park, southern Nevada: Geological Society of America Bulletin, v. 116, p. 42–59, doi: 10.1130/B25282.1.

Flodin, E.A., Aydin, A., Durlofsky, L.J., and Yeten, B., 2001, Representation of fault zone permeability in reservoir flow models: SPE paper 71671, presented at the Society of Petroleum Engineers Annual Technical Conference and Exhibition, New Orleans, 10 p.

Flodin, E.A., Prasad, M., and Aydin, A., 2003, Petrophysical constraints on deformation styles in Aztec Sandstone: Pure and Applied Geophysics, v. 160, p. 1589–1610.

Flodin, E.A., Gerdes, M., Aydin, A., and Wiggins, W.D., 2005, Petrophysical properties and sealing capacity of fault rock, Aztec Sandstone, Nevada, *in* Sorkhabi, R., and Tsuji, Y., eds., Faults, fluid flow, and petroleum traps: American Association for Petroleum Geologists Memoir, v. 85, p. 197–217.

Gale, J.F.W., Laubach, S.E., Marrett, R.A., Olson, J.E., Holder, J., and Reed, R.M., 2004, Predicting and characterizing fractures in dolostone reservoirs: Using the link between diagenesis and fracturing, *in* Braithwaite, C.J.R., Rizzi, G., and Darke, G., eds., The geometry and petrogenesis of dolomite hydrocarbon reservoirs: London, Geological Society Special Publication 235, p. 177–192.

Gross, M.R., 1995, Fracture partitioning: Failure mode as a function of lithology in the Monterey Formation of coastal California: Geological Society of America Bulletin, v. 107, p. 779–792, doi: 10.1130/0016-7606(1995)107<0779:FPFMAA>2.3.CO;2.

Hill, R.E., 1989, Analysis of deformation bands in the Aztec Sandstone, Valley of Fire State Park, Nevada [M.S. thesis]: Las Vegas, University of Nevada, 68 p.

Jourde, H., Flodin, E.A., Aydin, A., Durlofsky, L.J., and Wen, X.-H., 2002, Computing permeability of fault zones in aeolian sandstone from outcrop measurements: AAPG Bulletin, v. 86, p. 1187–1200.

Kattenhorn, S.A., Aydin, A., and Pollard, D.D., 2000, Joints at high angles to normal fault strike: An explanation using 3-D numerical models of fault-perturbed stress fields: Journal of Structural Geology, v. 22, p. 1–23, doi: 10.1016/S0191-8141(99)00130-3.

Laubach, S.E., Reed, R.M., Olson, J.E., Lander, R.H., and Bonnell, L.M., 2004, Coevolution of crack-seal texture and fracture porosity in sedimentary rocks: Cathodoluminescence observations of regional fractures: Journal of Structural Geology, v. 26, p. 967–982, doi: 10.1016/j.jsg.2003.08.019.

Lin, P., and Logan, J.M., 1991, The interaction of two closely spaced cracks: A rock model study: Journal of Geophysical Research, v. 96, p. 21,667–21,675.

Longwell, C.R., 1949, Structure of the northern Muddy Mountain area, Nevada: Geological Society of America Bulletin, v. 60, p. 923–967.

Martel, S.J., 1990, Formation of compound strike-slip fault zones, Mount Abbot quadrangle, California: Journal of Structural Geology, v. 12, p. 869–882, doi: 10.1016/0191-8141(90)90060-C.

Marzolf, J., 1983, Changing wind and hydraulic regimes during deposition of the Navajo and Aztec sandstones, Jurassic (?) southwestern United States, *in* Brookfield, M.E., and Ahlbrandt, T.S., eds., Eolian sediments and processes: Amsterdam, Elsevier, p. 635–660.

Marzolf, J.E., 1990, Reconstruction of extensionally dismembered early Mesozoic sedimentary basins; Southwestern Colorado Plateau to the eastern Mojave Desert, *in* Wernicke, B.P., ed., Basin and Range extensional tectonics near the latitude of Las Vegas, Nevada: Geological Society of America Memoir 176, p. 477–500.

Mollema, P.N., and Antonellini, M.A., 1996, Compaction bands: a structural analog for anti-mode I cracks in aeolian sandstone: Tectonophysics, v. 267, p. 209–228, doi: 10.1016/S0040-1951(96)00098-4.

Munsell Soil Color Charts, 1994, revised edition: New Windsor, New York, Munsell Color, 10 p.

Myers, R.D., 1999, Structure and hydraulics of brittle faults in sandstone [Ph.D. thesis]: Stanford, Stanford University, 176 p.

Myers, R.D., and Aydin, A., 2004, The evolution of faults formed by shearing across joint zones in sandstone: Journal of Structural Geology, v. 26, p. 947–966, doi: 10.1016/j.jsg.2003.07.008.

Nicholson, C., Seeber, L., Williams, P., and Sykes, L.R., 1986, Seismic evidence for conjugate slip and block rotation within the San Andreas fault system, southern California: Tectonics, v. 5, p. 629–648.

Nur, A., Ron, H., and Scotti, O., 1986, Fault mechanics and the kinematics of block rotations: Geology, v. 14, p. 746–749, doi: 10.1130/0091-7613(1986)14<746:FMATKO>2.0.CO;2.

Peacock, D.C.P., 2001, The temporal relationship between joints and faults: Journal of Structural Geology, v. 23, p. 329–341, doi: 10.1016/S0191-8141(00)00099-7.

Poole, F.G., 1964, Paleowinds in the western United States, *in* Nairn, A.E.M., ed., Problems in paleoclimatology: London, John Wiley, p. 394–406.

Rock-Color Chart Committee, 1970, Rock-color chart, reprint: Boulder, Colorado, Geological Society of America, 16 p.

Segall, P., and Pollard, D.D., 1980, Mechanics of discontinuous faults: Journal of Geophysical Research, v. 85, p. 4337–4350.

Sigda, J.M., Goodwin, L.B., Mozley, P.S., and Wilson, J.L., 1999, Permeability alteration in small-displacement faults in poorly lithified sediments: Rio Grande Rift, Central New Mexico, *in* Haneberg, W.C., Mozley, P.S., Moore, J.C., and Goodwin, L.B., eds., Faults and Subsurface fluid flow in the shallow crust: Geophysical Monograph, v. 113, Washington D.C., American Geophysical Union, p. 51–68.

Sternlof, K., Chapin, J.R., Pollard, D.D., and Durlofsky, L.J., 2004, Permeability effects of deformation band arrays in sandstone: AAPG Bulletin, v. 88, p. 1315–1329, doi: 10.1306/03280403103.

Sternlof, K., and Pollard, D.D., 2001, Deformation bands as linear elastic fractures: progress in theory and observation: Eos (Transactions, American Geophysical Union), v. 82, no. 47, Fall Meeting Supplement, Abstract T42E-04.

Taylor, W.L., 1999, Fluid flow and chemical alteration in fractured sandstones [Ph.D. thesis]: Stanford, California, Stanford University, 411 p.

Taylor, W.L., and Pollard, D.D., 2000, Estimation of in situ permeability of deformation bands in porous sandstone, Valley of Fire, Nevada: Water Resources Research, v. 36, p. 2595–2606, doi: 10.1029/2000WR900120.

Taylor, W.L., Pollard, D.D., and Aydin, A., 1999, Fluid flow in discrete joint sets: Field observations and numerical simulations: Journal of Geophysical Research, v. 104, p. 28983–29006, doi: 10.1029/1999JB900179.

Worden, R.H., and Morad, S., 2000, Quartz cementation in oil field sandstones: a review of key controversies, *in* Worden, R.H., and Morad, S., eds., Quartz cementation in sandstones: International Association of Sedimentologists Special Publication no. 29: Oxford, UK, Blackwell Science, p. 1–20.

Worden, R.H., and Morad, S., 2003, Clay minerals in sandstones: controls on formation, distribution and evolution, *in* Worden, R.H., and Morad, S., eds., Clay mineral cements in sandstones: International Association of Sedimentologists Special Publication no. 34: Oxford, UK, Blackwell Science, p. 3–41.

Printed in the USA